

See discussions, stats, and author profiles for this publication at: <https://www.researchgate.net/publication/235573000>

# Effect of Sparger Design and Height to Diameter Ratio on Fractional Gas Hold-up in Bubble Columns

Article in *Chemical Engineering Research and Design* · October 1998

DOI: 10.1205/026387698525577

---

CITATIONS

102

---

READS

3,252

9 authors, including:



**Bhaskar Thorat**

Institute of Chemical Technology

172 PUBLICATIONS 3,122 CITATIONS

SEE PROFILE



**Ravindra Aglave**

Siemens USA

72 PUBLICATIONS 368 CITATIONS

SEE PROFILE



**Shirish Thakre**

Aditya Birla Group

32 PUBLICATIONS 731 CITATIONS

SEE PROFILE



**Aniruddha Bhalchandra Pandit**

Institute of Chemical Technology

573 PUBLICATIONS 32,473 CITATIONS

SEE PROFILE

# EFFECT OF SPARGER DESIGN AND HEIGHT TO DIAMETER RATIO ON FRACTIONAL GAS HOLD-UP IN BUBBLE COLUMNS

B. N. THORAT, A. V. SHEVADE, K. N. BHILEGAONKAR, R. H. AGLAWE, U. PARASU VEERA, S. S. THAKRE, A. B. PANDIT, S. B. SAWANT and J. B. JOSHI

*Department of Chemical Technology, University of Mumbai, Matunga, India*

The combined effect of sparger design and dispersion height on fractional gas hold-up ( $\bar{\epsilon}_G$ ) was investigated in a 0.385 m i.d. bubble column. Perforated plates were used as spargers. Free areas of sparger plates (F.A.) and hole diameters were varied in the range of 0.13% to 5.0% and 0.8 mm to 87 mm, respectively. The height to diameter ratio ( $H_D/D$ ) was varied in the range of 1–8. In all the cases, the superficial gas velocity was covered in the range of 30–300 mm s<sup>-1</sup>. In order to investigate the combined effects of sparger design and the  $H_D/D$  ratio together with the coalescing nature of the liquid phase, three liquid systems were considered, namely, water, an aqueous solution of an electrolyte and an aqueous solution of carboxymethyl cellulose (CMC). The comparative behaviour of these systems has been presented. The effects of sparger design,  $H_D/D$  ratio and the gas-liquid system have also been analysed on the basis of drift flux model. A predictive procedure has been given for the drift flux constants by simulating the flow pattern in bubble columns using Computational Fluid Dynamics (CFD).

*Keywords: bubble column; gas hold-up; sparger design; aspect ratio; non-Newtonian liquids; non-coalescing liquid*

## INTRODUCTION

Facile construction and low costs make bubble columns highly attractive gas-liquid contactors. Their use as absorbers, fermenters, catalytic reactors, coal liquifiers, soakers, etc., is widespread and extensive. Fractional gas hold-up ( $\bar{\epsilon}_G$ ) is an important parameter in the design and scale-up of bubble column reactors. It has several direct and indirect influences on the column performance. The direct and obvious effect is on the column volume. This is because the fraction of the volume is occupied by the gas and the respective phase volume becomes important depending upon the phase in which the rate controlling step takes place. The indirect influences are far reaching. The spatial variation of  $\bar{\epsilon}_G$ , gives rise to pressure variation and eventually results in intense liquid phase motion. These secondary motions govern the rate of mixing, heat transfer and mass transfer. Fortunately, the radial distribution of  $\bar{\epsilon}_G$  can be estimated through the knowledge of the  $\bar{\epsilon}_G - V_G$  relationship which can be conveniently established experimentally.

The gas phase moves in one of the two characteristic regimes depending upon the nature of dispersion. These are called homogeneous (or bubbly flow) and heterogeneous (or churn turbulent) regimes. The homogeneous regime is characterized by uniform sized bubbles. Further, the concentration of bubbles is also uniform, particularly in the transverse direction. The process of coalescence and dispersion are practically absent in the homogeneous regime

and hence the sizes of bubbles are entirely dictated by the sparger design and the physical properties of the gas and liquid phases. In contrast, in the heterogeneous regime, the role of sparger design diminishes depending upon the column height. In fact, the total column height can be divided into two regions: the sparger region and the bulk region. The size of the bubble formed at the sparger (primary bubble size,  $d_{BP}$ ) depends upon the sparger design, the local energy dissipation rate and the surface active contaminants. The value  $d_{BP}$  decreases with an increase in the energy dissipation rate. Under otherwise similar conditions of  $d_o$ ,  $\sigma$ ,  $\rho_L$ ,  $\rho_G$ ,  $\mu_L$ , etc., smaller bubbles are formed in the presence of surface active contaminant such as an electrolyte.

In the sparger region, the bubble size changes with respect to height depending upon the coalescence nature of the liquid phase, the extent of turbulence and the bulk motion. At the end of the sparger region, the bubbles attain an equilibrium size (called secondary bubble size,  $d_{BS}$ ). The equilibrium is governed by the breaking forces due to bulk motion (turbulent and viscous stresses) and the retaining force due to surface tension.

The height of the sparger region depends upon the difference between  $d_{BP}$  and  $d_{BS}$ , the coalescing nature of the liquid phase and the liquid circulation in the heterogeneous regime. The relative proportion of the sparger region in the total column height decides the effect of  $H_D/D$  ratio on  $\bar{\epsilon}_G$ . If the sparger region is small, the effect of  $H_D/D$  ratio on  $\bar{\epsilon}_G$  is minimum and vice-versa.

The fractional gas hold-up in bubble columns has been extensively investigated during the last fifty years and more than 200 papers are available in the published literature. As regards to the effect of the  $H_D/D$  ratio on  $\bar{\epsilon}_G$ , the following observations were noted from the published literature

(i) in the majority of papers where the sparger design and  $H_D/D$  ratio were found to be important, the major impact was due to the transition from homogeneous to heterogeneous regime and vice-versa. This was principally because of the selection of small diameter columns (<150 mm) and the lower range of superficial gas velocity<sup>1-9</sup> (<100 mm s<sup>-1</sup>),

(ii) in another set of papers, where the heterogeneous regime was ensured ( $D > 150$  mm,  $V_G > 50$  mm s<sup>-1</sup>), the height to diameter ratio was also larger than five. Under these conditions, the influence of sparger design gets more or less eliminated<sup>4,6-15</sup>.

In this paper, an attempt has been made to investigate the role of sparger design and the  $H_D/D$  ratio together with the coalescing nature of liquid phase. There are several examples of industrial importance where the height to diameter ratio is smaller than five.

## EXPERIMENTAL

Experiments were carried out in a perspex cylindrical bubble column of 385 mm i.d. and 3.2 m height. A schematic diagram is shown in Figure 1. Sieve plate spargers were placed between the column and distribution chamber having a drain at the bottom and gas inlet at the side. A U-tube manometer was used to measure the pressure drop across the sparger. The clear liquid height was measured using a side tube. A perspex chamber with a vent was introduced, as shown in Figure 1, to disengage the bubbles passing into the side tube, thus reducing the error introduced due to fluctuations in the level. Sieve plates

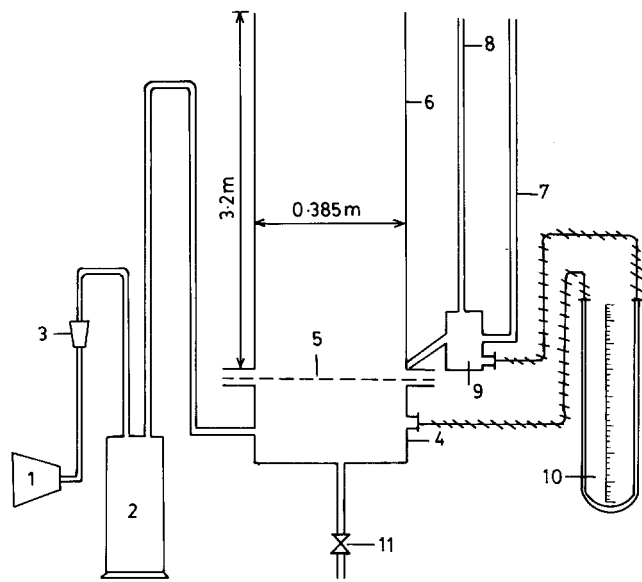


Figure 1. Experimental setup. 1 Air compressor; 2 Surge vessel; 3 Rotameter; 4 Distribution chamber; 5 Sparger; 6 Bubble column; 7 Clear liquid tube; 8 Vent; 9 Disengaging chamber; 10 Manometer; 11 Drain valve.

Table 1. Design details of sieve-plate spargers.

Name	$d_o$	$N$	Pitch, LP	%F.A
SP1	0.8	315	Triangular	
SP2	1.5	88	Triangular	
SP3	3	23	Triangular	0.13
SP4	6	6	Triangular	
SP5	10	2	—	
SP6	14	1	—	
SP7	1.5	132	Triangular	0.2
SP8	3	33	Triangular	
SP9	1.5	198	Triangular	0.3
SP10	3	50	Triangular	
SP11	1	623	Random	
SP12	1.5	269	Triangular	
SP13	3	71	Triangular	0.42
SP14	6	16	Triangular	
SP15	25	1	—	
SP16	2.5	330	Random	
SP17	4	156	Triangular	1.68
SP18	6	64	Triangular	
SP19	50	1	—	
SP20	3	823	Random	
SP21	6	210	Random	5
SP22	87	1	—	

were used as spargers. Twenty-two different spargers were employed with hole diameters in the range of 0.8 to 87 mm and percent free area was in the range of 0.13 to 5%. Further details of the sparger are given in Table 1. Three systems were used, namely, air-water, air-aqueous solution of 1% CMC (Sodium-salt) and air-electrolyte solution (NaCl). The  $H_D/D$  ratio was varied in the range of 1–8 and the superficial gas velocity in the range of 0–300 mm s<sup>-1</sup>. The liquid phase temperature was  $30 \pm 3^\circ\text{C}$ .

Experiments were carried out starting with the highest  $V_G$  and the highest  $H_D/D$ . The air flow rate was measured using a pre-calibrated rotameter. As  $V_G$  decreases (for instance, at  $H_D/D = 8$ ), the dispersion height ( $H_D$ ) also decreases. The value of  $H_D$  was maintained by adding liquid into the column thereby increasing the clear liquid height. The same procedure was repeated at each  $H_D/D$  ratio, running down from 8 to 1. The fractional gas hold-up was then calculated as  $(H_D - H)/H_D$ .

## RESULTS AND DISCUSSION

### Air-Water System

#### Effect of $H_D/D$ ratio

For multipoint spargers having  $d_o < 3$  mm, the fractional gas hold-up ( $\bar{\epsilon}_G$ ) was seen to be maximum at  $H_D/D = 1$  and decreased by 15–20% as  $H_D/D$  increased up to a value of 4 to 5. A further increase in  $H_D/D$  ratio results into a marginal decrease in  $\bar{\epsilon}_G$ . However, a still higher ratio was found to have no effect on  $\bar{\epsilon}_G$ . Typical cases are shown in Figures 2A and 2B. For the spargers having  $d_o < 3$  mm the bubbles generated at the spargers ( $d_{BP}$ ) are smaller than the equilibrium bubble size in the bulk ( $d_{BS}$ ). With an increase in the  $H_D/D$  ratio, the bubble size increases as a result of coalescence/dispersion and perhaps attains the equilibrium bubble size when  $H_D/D = 5$ . In case of  $d_o \geq 3$  (3–6 mm) there was practically no effect of the  $H_D/D$  ratio on  $\bar{\epsilon}_G$ , as shown in Figures 2C and 2D. The probable reason for this could be that the bubbles generated have a size very similar to the equilibrium bubble size.

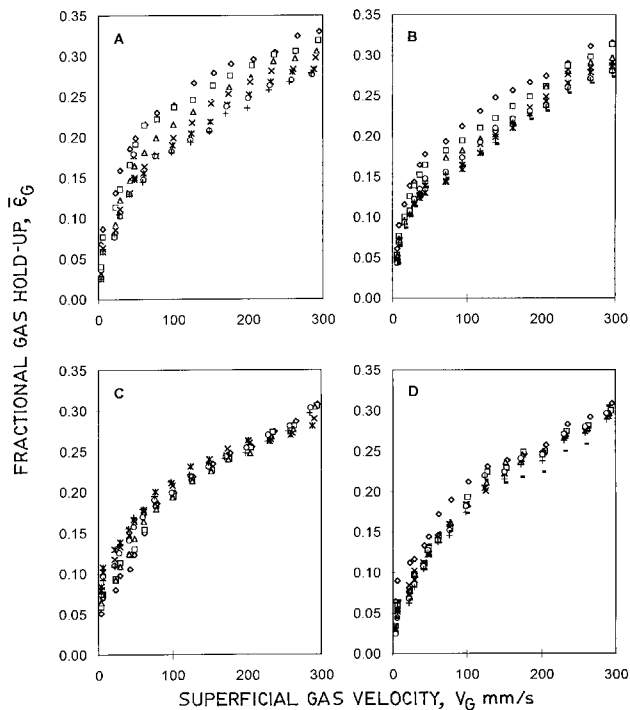


Figure 2. Fractional gas hold-up ( $\bar{\epsilon}_g$ ) versus superficial gas velocity ( $V_g$ ) with dispersion height ( $H_d/D$ ) as a parameter for various sparger plate designs: (A) SP11, (B) SP12 (C) SP13 (D) SP14;  $\diamond$   $H_d/D = 1$ ,  $\square$   $H_d/D = 2$ ,  $\triangle$   $H_d/D = 3$ ,  $\times$   $H_d/D = 4$ ,  $*$   $H_d/D = 5$ ,  $\circ$   $H_d/D = 6$ ,  $+$   $H_d/D = 7$ ,  $-$   $H_d/D = 8$ .

In the case of singlepoint spargers, a reverse trend was observed, as shown in Figures 3A and 3B. For all singlepoint spargers, the size of primary bubble is large together with high bubble rise velocity. At low  $H_d/D$ , these bubbles disengage very fast. However, as the  $H_d/D$  increases, the bubbles get sufficient time to disintegrate into small bubbles. This leads to an increase in the average gas hold-up by about 50–100% at  $H_d/D = 5$ . However above a dispersion height of 4–5, the bubbles reach the equilibrium size and a minimum increase in the average gas hold-up was seen with further increase in the  $H_d/D$  ratio.

#### Effect of hole diameter

The effect of hole diameter with respect to the  $H_d/D$  ratio is shown in Figure 4. It can be seen from Figures 4A–4D that when  $d_o < 3$  mm,  $\bar{\epsilon}_g$  decreases with an increase in the  $H_d/D$  ratio. For  $d_o = 3$ –6 mm, the effect is minimum. However for single point spargers,  $\bar{\epsilon}_g$  increases with an increase in the  $H_d/D$  ratio. Thus the effect of hole diameter is maximum at  $H_d/D = 1$  and the effect practically vanishes when  $H_d/D > 5$ . Further, at  $H_d/D = 1$ , the effect of the hole diameter was found to increase with a decrease in free area.

The combined effect of the  $H_d/D$  ratio and the hole diameter which was shown in Figures 2 to 4 can further be explained on the basis of the gas hold-up profile, as shown in Figure 5. In the case of a singlepoint sparger, as shown in Figure 5A, a gas jet issues at the centre. The gas hold-up profile is very steep (at  $h = 0$ , the gas jet is at the centre and there is a bubble free region up to the wall). As the bubbles rise, they move radially outward due to turbulent dispersion. As a result, the hold-up profile becomes continuously less steep with an increase in  $H_d/D$ . At  $H_d/D > 5$ , the hold-up

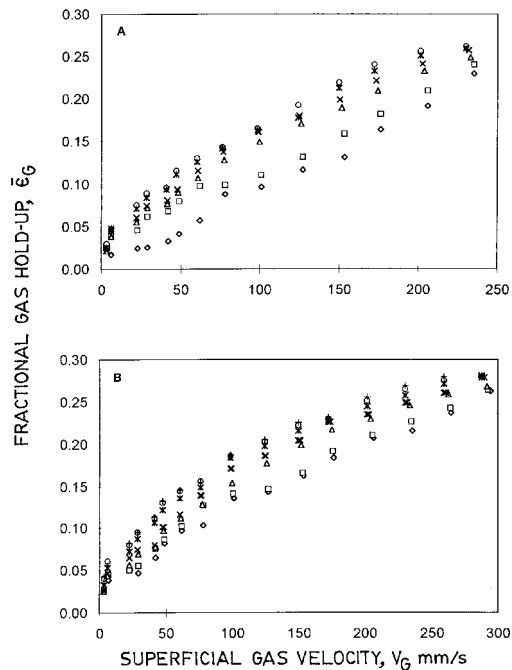


Figure 3. Fractional gas hold-up ( $\bar{\epsilon}_g$ ) versus superficial gas velocity ( $V_g$ ) for single point spargers, with dispersion height ( $H_d/D$ ) as a parameter. (A) SP6 (B) SP15;  $\diamond$   $H_d/D = 1$ ,  $\square$   $H_d/D = 2$ ,  $\triangle$   $H_d/D = 3$ ,  $\times$   $H_d/D = 4$ ,  $*$   $H_d/D = 5$ ,  $\circ$   $H_d/D = 6$ ,  $+$   $H_d/D = 7$ .

profile is fully developed and has a parabolic shape. It can also be said that the contribution of the bubble free region to the overall  $\bar{\epsilon}_g$  decreases with an increase in  $H_d/D$ . Therefore, the value of  $\bar{\epsilon}_g$  increases with an increase in the  $H_d/D$  ratio.

For a multipoint sparger, at  $h = 0$ , the gas hold-up profile is uniform, as shown in Figure 5B. The gas bubbles move radially inwards due to liquid circulation and finally at  $H_d/D > 5$ , the hold-up profile is fully developed. Therefore, the value of  $\bar{\epsilon}_g$  decreases with an increase in the  $H_d/D$  ratio.

The contribution of liquid circulation on the development of the hold-up profile will now be explained. In fact, the liquid circulation and the gas hold-up profile are strongly interrelated and develop together. The liquid circulation is upward where the gas hold-up is greater and that is in the central region. Therefore, the overall bubble rise velocity is higher in the central region where the gas concentration is also high. As a result, the liquid circulation reduces the residence time of the gas phase and hence the gas hold-up. An approximate equation for the liquid circulation velocity ( $V_c$ ) can be established on the basis of the pressure driving force generated due to the hold-up profile. If  $\Delta\epsilon_g$  is the average hold-up difference between the central and the near wall region,  $V_c$  is given by the following expression:

$$V_c \propto (\Delta\epsilon_g g H)^{1/2} \quad (1)$$

It can be seen from Figure 5A that the value of  $\Delta\epsilon_g$  decreases with an increase in the height of dispersion ( $H_d$ ) for a singlepoint sparger. In contrast, for multipoint spargers,  $\Delta\epsilon_g$  increases with an increase in the height of dispersion (Figure 5B). Therefore, the liquid circulation intensifies at a faster rate (with  $H_d$ ) for multipoint spargers as compared to that in the singlepoint sparger. As a consequence, in the case of multipoint spargers, the gas

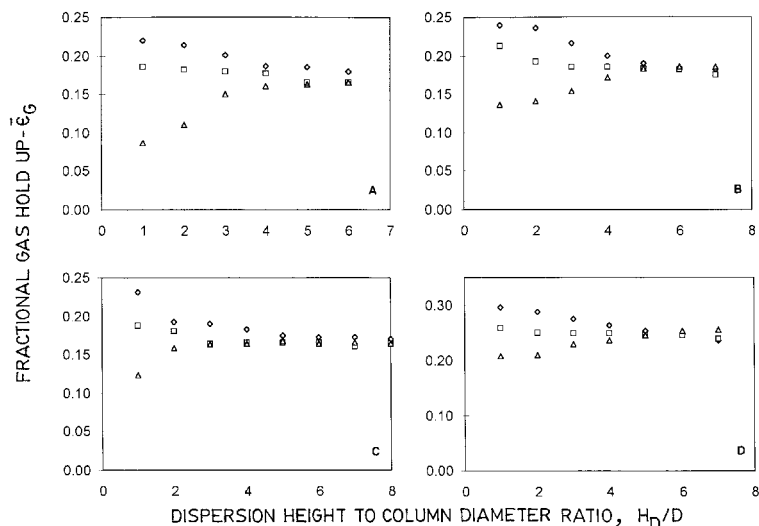


Figure 4. Fractional gas hold-up ( $\bar{\epsilon}_G$ ) versus dispersion height to column diameter ratio ( $H_D/D$ ) with hole diameter as a parameter for various sparger designs;  $V_G$  as a parameter (A)  $\%F.A. = 0.135$ ,  $V_G = 100 \pm 3 \text{ mm s}^{-1}$ :  $\diamond$   $d_o = 0.8 \text{ mm}$ ,  $\square$   $d_o = 6 \text{ mm}$ ,  $\triangle$   $d_o = 14 \text{ mm}$ ; (B)  $\%F.A. = 0.42$ ,  $V_G = 100 \pm 3 \text{ mm s}^{-1}$ :  $\diamond$   $d_o = 1 \text{ mm}$ ,  $\square$   $d_o = 6 \text{ mm}$ ,  $\triangle$   $d_o = 25 \text{ mm}$ ; (C)  $\%F.A. = 1.68\%$ ,  $V_G = 100 \pm 3 \text{ mm s}^{-1}$ :  $\diamond$   $d_o = 2.5 \text{ mm}$ ,  $\square$   $d_o = 6 \text{ mm}$ ,  $\triangle$   $d_o = 50 \text{ mm}$  (D)  $\%F.A. = 0.42\%$ ,  $V_G = 203 \pm 3 \text{ mm s}^{-1}$ :  $\diamond$   $d_o = 1 \text{ mm}$ ,  $\square$   $d_o = 6 \text{ mm}$ ,  $\triangle$   $d_o = 25 \text{ mm}$ .

phase residence time and hence the value of  $\bar{\epsilon}_G$  decreases with an increase in the  $H_D/D$  ratio.

#### Effect of free area

The effect of free area for multipoint spargers was found to be nominal for the range of parameters covered in this work, as can be seen from Figures 6A–6C. For  $d_o < 3 \text{ mm}$  and  $d_o = 3 \text{ mm}$ , no effect of free area on  $\bar{\epsilon}_G$  is observed (Figure 6A and 6B; to avoid the clustering of data, two Y-axis scales have been used). For spargers with  $d_o = 6 \text{ mm}$ ,  $\bar{\epsilon}_G$  was found to decrease marginally by about 8 to 10% with an increase in the free area from 0.42% to 1.68%. Similar observations were made at both  $H_D/D$  values of 1 and 5 (Figure 6C). The probable reason for this could be an uneven distribution of gas through the sparger with higher free area over the given range of  $V_G$ .

For singlepoint spargers, Figure 6D does not show any trend with respect to the effect of % free area especially at  $H_D/D = 1$ . There appears to be a possibility of an optimum value of free area (0.42%). However, at  $H_D/D = 5$ , no systematic trend was observed. At a given superficial gas velocity the  $\bar{\epsilon}_G$  values were found to be within 12%.

#### Air-Aqueous Solution of Electrolyte

In the previous section, the combined effect of the sparger design and  $H_D/D$  ratio was presented for the air-water system. It is important to understand the combined effect with respect to the coalescing nature of the liquid phase. In order to reduce the coalescing nature with respect to water, aqueous solutions of electrolyte were employed.

Recently, Zahradnik *et al.*<sup>16</sup> have presented a systematic investigation considering various electrolyte solutions over a wide range of concentrations. For all the electrolyte solutions, they have shown that the value of  $\bar{\epsilon}_G$  increases with an increase in electrolyte concentration. However, the effect of concentration levels off at a certain critical concentration. This means that the non-coalescing property of the electrolyte reaches its limiting value at the critical

concentration. Therefore, in the present work, it was thought desirable to use an electrolyte concentration slightly above the critical value. Aqueous sodium chloride solution has been used at 0.2 M (critical concentration = 0.145 M).

The effects of sparger design and the  $H_D/D$  ratio are

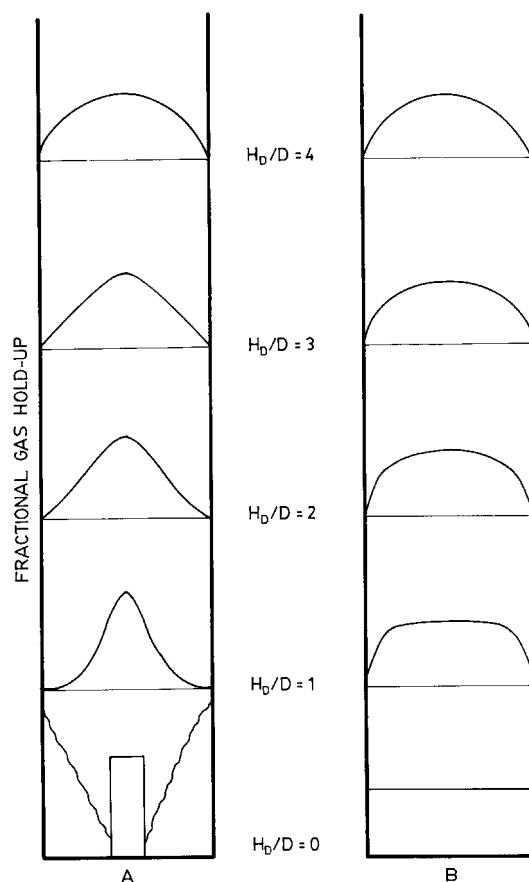


Figure 5. Schematic representation of the development of hold-up profiles for (A) single point spargers and (B) multipoint spargers.

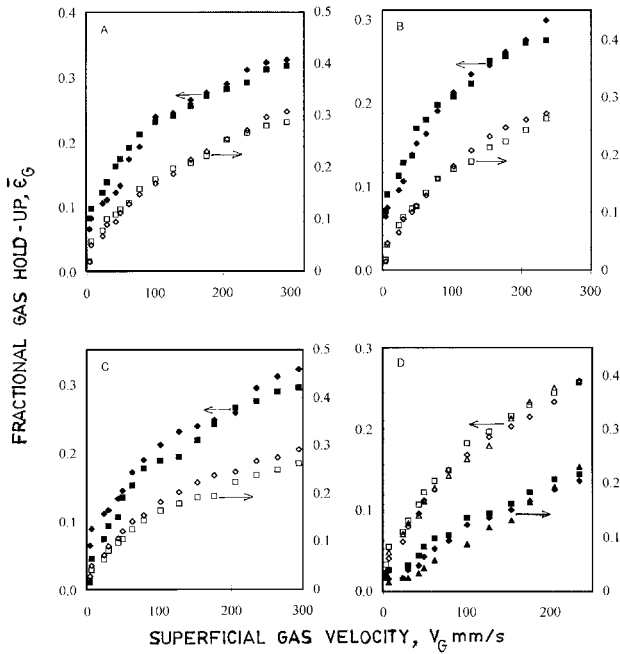


Figure 6. Fractional gas hold-up ( $\bar{\epsilon}_G$ ) versus superficial gas velocity ( $V_G$ ) with %F.A. as a parameter (A) for  $d_o = 1.5$  mm,  $H_D/D = 1$ :  $\diamond$  %F.A. = 0.135%,  $\square$  %F.A. = 0.42%;  $H_D/D = 5$ :  $\diamond$  %F.A. = 0.135%,  $\square$  %F.A. = 0.42%, (B) for  $d_o = 3$  mm,  $H_D/D = 1$ :  $\diamond$  %F.A. = 0.135%,  $\square$  %F.A. = 0.42%;  $H_D/D = 5$ : %F.A. = 0.135%,  $\square$  %F.A. = 0.42%, (C) for  $d_o = 6$  mm,  $H_D/D = 1$ :  $\diamond$  %F.A. = 0.42%,  $\square$  %F.A. = 1.68%;  $H_D/D = 5$ :  $\diamond$  %F.A. = 0.42%,  $\square$  %F.A. = 1.68%, (D) for single point spargers  $H_D/D = 1$ :  $\triangle$  %F.A. = 0.135%,  $\square$  %F.A. = 0.42%,  $\diamond$  %F.A. = 1.68%;  $H_D/D = 5$ : %F.A. = 0.135%,  $\square$  %F.A. = 0.42%,  $\diamond$  %F.A. = 1.68%.

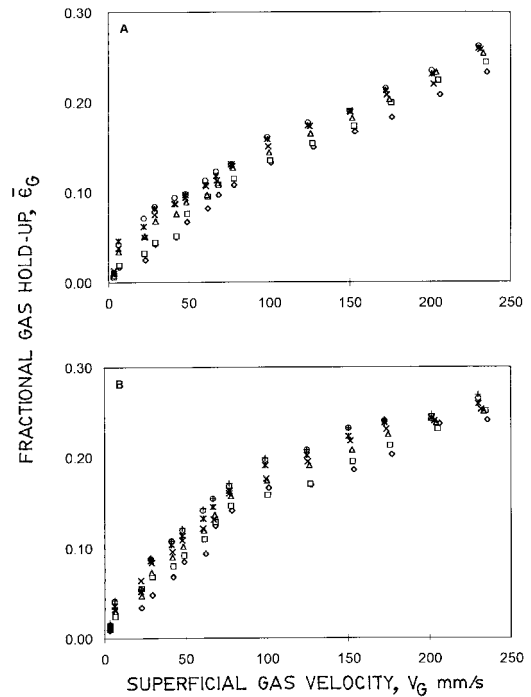


Figure 8.  $\bar{\epsilon}_G$  versus  $V_G$  for single point spargers, with  $H_D/D$  as a parameter for air-electrolyte system. (A) SP6 (B) SP15.  $\diamond$   $H_D/D = 1$ ,  $\square$   $H_D/D = 2$ ,  $\triangle$   $H_D/D = 3$ ,  $\times$   $H_D/D = 4$ ,  $*$   $H_D/D = 5$ ,  $\circ$   $H_D/D = 6$ .

shown in Figures 7 to 9. The behaviour of  $\bar{\epsilon}_G$  is qualitatively similar to that for air-water system, as shown in Figures 7 and 8. However, one can note several distinctive features as compared to the air-water system:

- (i) In both the cases, the  $\bar{\epsilon}_G$  changes with respect to the  $H_D/D$  ratio up to a certain ratio and then it levels off (equilibrium hold-up). The equilibrium hold-up was found to be independent of the sparger design in both the cases. However, the equilibrium hold-up value was found to be 15–20% higher for electrolyte solution as compared to air-water system.
- (ii) It is known that the bubble size generated at the sparger is smaller in the case of an electrolyte solution as compared to that in air-water system. Therefore, at  $H_D/D = 0$  itself,  $\bar{\epsilon}_G$  is expected to be much higher than the air-water system.
- (iii) For multipoint as well as single point spargers, the variation of  $\bar{\epsilon}_G$  with respect to  $H_D/D$  is slower (Figure 9) as compared to the variation in the air-water system (Figure 5). For instance, in electrolyte solutions, the variations for multipoint and singlepoint spargers were found to be 10–12% and 10–15%, respectively. Whereas, these numbers for the air-water system were 20–22% and 50–100%, respectively.
- (iv) From Figures 2 to 4 and 6 to 9 it can be observed that the effect of  $H_D/D$  levels off at a ratio 5 for the air-water system. Whereas, in electrolyte solutions the ratio extends up to 8. In some cases (Figure 9C) the variation was found to be even slower.

#### Air-Aqueous Solution of Carboxymethyl Cellulose

The fractional gas hold-up value for highly viscous pseudoplastic carboxymethyl cellulose (CMC) solution was measured against superficial gas velocity under the

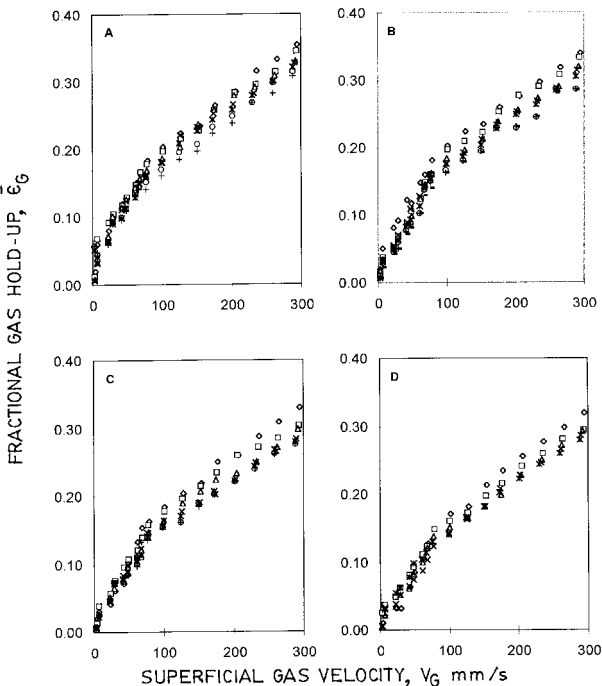


Figure 7.  $\bar{\epsilon}_G$  versus  $V_G$  with  $H_D/D$  as a parameter for air-electrolyte system: (A) SP11, (B) SP12, (C) SP13, (D) SP14.  $\diamond$   $H_D/D = 1$ ,  $\square$   $H_D/D = 2$ ,  $\triangle$   $H_D/D = 3$ ,  $\times$   $H_D/D = 4$ ,  $*$   $H_D/D = 5$ ,  $\circ$   $H_D/D = 6$ ,  $+$   $H_D/D = 7$ .

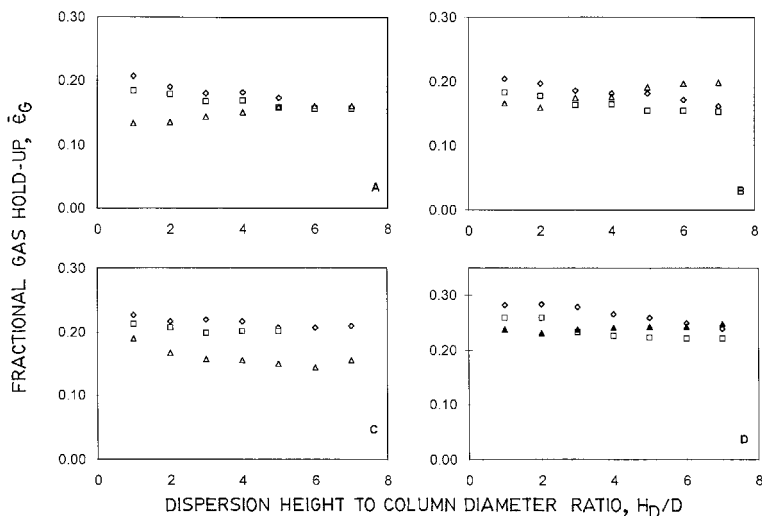


Figure 9.  $\bar{\varepsilon}_G$  versus  $H_D/D$  with  $d_o$  as a parameter for air-electrolyte system and at a particular  $V_G$ , viz. (A) %F.A. = 0.135,  $V_G = 100 \pm 3 \text{ mm s}^{-1}$ :  $\diamond d_o = 0.8 \text{ mm}$ ,  $\square d_o = 3 \text{ mm}$ ,  $\Delta d_o = 14 \text{ mm}$ ; (B) %F.A. = 0.42,  $V_G = 100 \pm 3 \text{ mm s}^{-1}$ :  $\diamond d_o = 1 \text{ mm}$ ,  $\square d_o = 3 \text{ mm}$ ,  $\Delta d_o = 25 \text{ mm}$ ; (C) %F.A. = 1.68%,  $V_G = 100 \pm 3 \text{ mm s}^{-1}$ :  $\diamond d_o = 2.5 \text{ mm}$ ,  $\square d_o = 4 \text{ mm}$ ,  $\Delta d_o = 6 \text{ mm}$  (D) %F.A. = 0.42%,  $V_G = 203 \pm 3 \text{ mm s}^{-1}$ :  $\diamond d_o = 1 \text{ mm}$ ,  $\square d_o = 3 \text{ mm}$ ,  $\Delta d_o = 25 \text{ mm}$ .

operating and design conditions similar to those for air-water and air-salt solution. The physical properties of 1% CMC solution were:  $n = 0.65$ ,  $k = 19.08 \text{ m Pa s}$ ,  $\rho_L = 1003 \text{ kg m}^{-3}$ . It was prepared by dissolving sodium salt of CMC powder (CEPOL, Cellulose Product of India Ltd.) in tap water.

#### Effect of $H_D/D$ ratio

Figures 10 and 11 show the effect of  $H_D/D$  on  $\bar{\varepsilon}_G$  for both multipoint and singlepoint spargers, respectively. The trends are similar to those for air-water and air-salt systems. However, the following differences were noted:

- (i) The value of equilibrium hold-up was found to be lower than the air-water system by 20–25%.
- (ii) For multipoint as well as for singlepoint spargers, the variation of  $\bar{\varepsilon}_G$  with respect to the  $H_D/D$  ratio was found to be faster (Figure 12) in the CMC solutions as compared to that in the air-water system, which in turn was found to be faster than that in electrolyte solutions. Thus the column height required for attaining equilibrium hold-up increases with an increase in the non-coalescing property of the liquid phase. For instance, the value of the limiting  $H_D/D$  ratio of air-CMC, air-water and air-electrolyte were found to be 3, 5 and 8, respectively.

#### Analysis of Hold-Up Data Using Drift Flux Model

##### Drift flux model

The drift flux model of Zuber and Findlay<sup>17</sup> is given by the following equation:

$$\frac{V_G}{\varepsilon_G} = C_0 V_G + C_1 \quad (2)$$

Where,  $C_0$  and  $C_1$  are the drift flux constants and are given by:

$$C_0 = \frac{\langle \varepsilon_G V_G \rangle}{\langle \varepsilon_G \rangle \langle V_G \rangle} \quad (3)$$

$$C_1 = \frac{\langle \varepsilon_G \varepsilon_L V_S \rangle}{\langle \varepsilon_G \rangle} \quad (4)$$

All the data presented in this work were analysed using equation (2).

Figure 13 shows the variation of  $C_1$  with respect to  $H_D/D$  for the air-water system. When the hole diameter is less than 1 mm, it can be seen that the value of  $C_1$  increases (though nominally) with respect to the  $H_D/D$  ratio. It levels off when the  $H_D/D$  ratio is about 5. It may be noted that

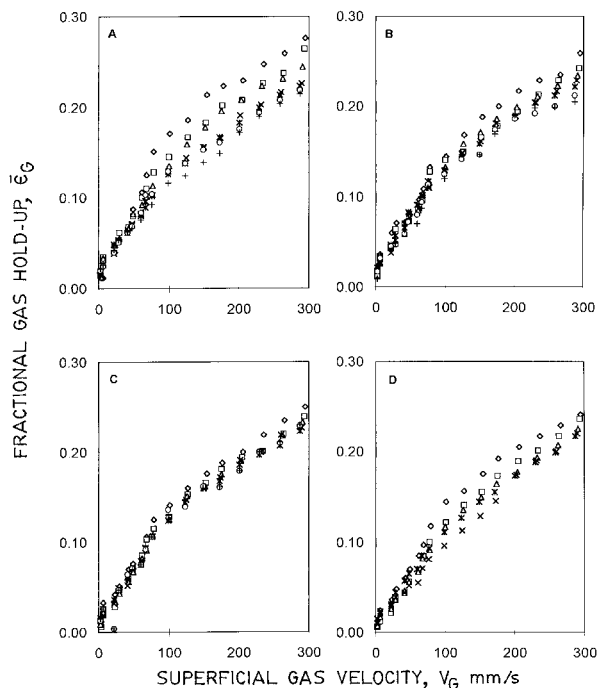


Figure 10.  $\bar{\varepsilon}_G$  versus  $V_G$  with  $H_D/D$  as a parameter for air-CMC system: (A) SP11, (B) SP12, (C) SP13, (D) SP14.  $\diamond H_D/D = 1$ ,  $\square H_D/D = 2$ ,  $\Delta H_D/D = 3$ ,  $\times H_D/D = 4$ ,  $* H_D/D = 5$ ,  $\circ H_D/D = 6$ ,  $+ H_D/D = 7$ .

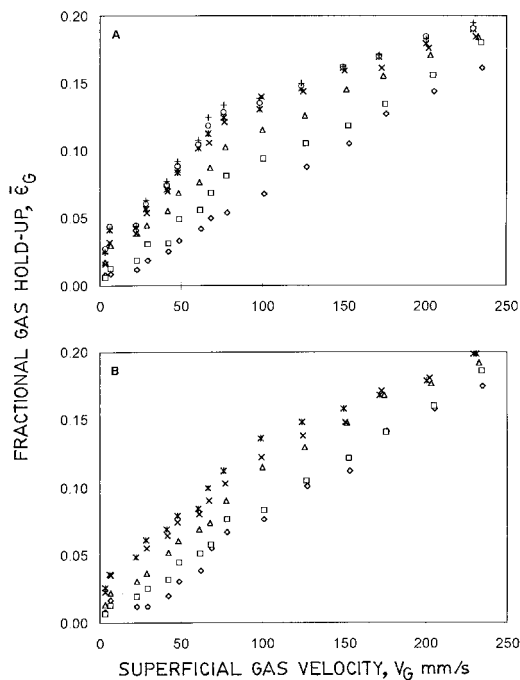


Figure 11.  $\bar{\epsilon}_G$  versus  $V_G$  for single point spargers, with  $H_D/D$  as a parameter for air-CMC system. (A) SP6, (B) SP15,  $\diamond$   $H_D/D = 1$ ,  $\square$   $H_D/D = 2$ ,  $\Delta$   $H_D/D = 3$ ,  $\times$   $H_D/D = 4$ ,  $*$   $H_D/D = 5$ .

the drift flux constant  $C_1$  represents the bubble rise velocity. Figure 13A shows that, when the hole diameter is less than 1 mm, small bubbles (with rise velocity less than  $200 \text{ mm s}^{-1}$ ) are produced. The bubbles grow as they ascend and reach a rise velocity of about  $300 \text{ mm s}^{-1}$  when  $H_D/D$  is 5.

In contrast to the above observation, Figure 13C shows that the value of  $C_1$  for single point spargers decreases with an increase in the  $H_D/D$  ratio. In the case of single point spargers, large bubbles are generated and the value of  $C_1$  is greater than  $700 \text{ mm s}^{-1}$  when  $H_D/D$  equals 1. The bubbles undergo break up and coalescence as they ascend to reach

an equilibrium bubble size when the  $H_D/D$  ratio is about 5. It may be pointed out that the value of  $C_1$  is practically the same for single as well as multipoint spargers when  $H_D/D$  is greater than 5.

For hole diameters in the range of 2.5 to 6 mm, the value of  $C_1$  can be seen to be independent of  $H_D/D$  (Figure 13B). Therefore, as pointed out earlier (for instance Figure 2C), the value of  $\bar{\epsilon}_G$  is independent of  $H_D/D$  ratio when the hole diameter is in the range of 2.5 to 6 mm.

The behaviour of other drift flux constants  $C_o$  has been shown in Figure 14. It can be seen that the value of  $C_o$  is practically independent of  $H_D/D$  ratio for all the spargers except the single point spargers. In the latter case, there is a slight increase in  $C_o$  in the  $H_D/D$  range of 1 to 3 (Figure 14C).

For the case of air- aqueous CMC system, the drift flux constants have been shown in Figure 15 and Figure 16. The trends are similar to those of air-water system. However, the values of  $C_o$  and  $C_1$  are higher for the case of CMC solution. It indicates that the bubble rise velocities are higher and the hold-up profiles are steeper for CMC solutions.

### Comparison of CFD and Experimental Data for Drift Flux Coefficients

A computational Fluid dynamic (CFD) code was developed for a two phase, two dimensional bubble column. A mathematical model was developed for the formulation of the governing equations of the flow variables and various interfacial forces between the gas and liquid. This represents a set of eight non-linear coupled equations, the details of which are given in Table 2. In the first step, equations of continuity and motion were solved (together with  $k - \epsilon$ ) for getting the complete flow pattern in terms of gas and liquid velocities, eddy diffusivity and gas hold-up.

A set of equations were solved numerically which consisted of the following steps:

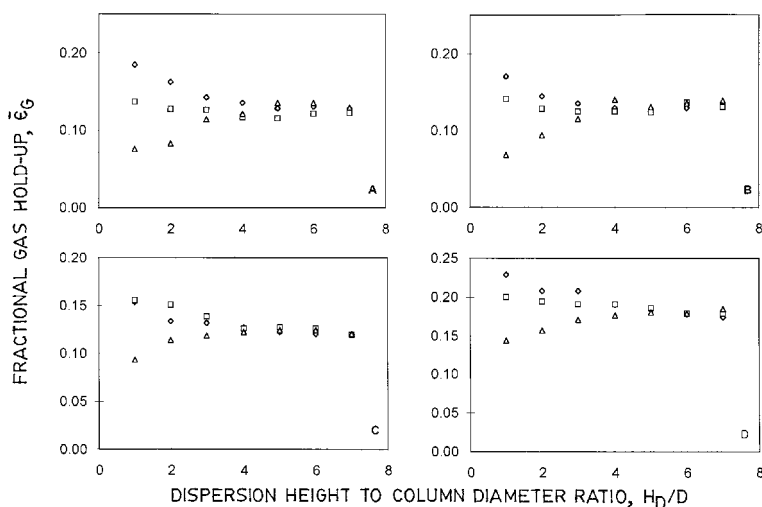


Figure 12.  $\bar{\epsilon}_G$  versus  $H_D/D$  with  $d_o$  as a parameter for air-CMC system and at a particular  $V_G$  viz. (A) %F.A. = 0.135,  $V_G = 100 \pm 3 \text{ mm s}^{-1}$ :  $\diamond$   $d_o = 0.8 \text{ mm}$ ,  $\square$   $d_o = 3 \text{ mm}$ ,  $\Delta$   $d_o = 14 \text{ mm}$ ; (B) %F.A. = 0.42,  $V_G = 100 \pm 3 \text{ mm s}^{-1}$ :  $\diamond$   $d_o = 1 \text{ mm}$ ,  $\square$   $d_o = 3 \text{ mm}$ ,  $\Delta$   $d_o = 25 \text{ mm}$ ; (C) %F.A. = 1.68%,  $V_G = 100 \pm 3 \text{ mm s}^{-1}$ :  $\diamond$   $d_o = 4 \text{ mm}$ ,  $\square$   $d_o = 6 \text{ mm}$ ,  $\Delta$   $d_o = 50 \text{ mm}$  (D) %F.A. = 0.42%,  $V_G = 203 \pm 3 \text{ mm s}^{-1}$ :  $\diamond$   $d_o = 1 \text{ mm}$ ,  $\square$   $d_o = 3 \text{ mm}$ ,  $\Delta$   $d_o = 25 \text{ mm}$ .

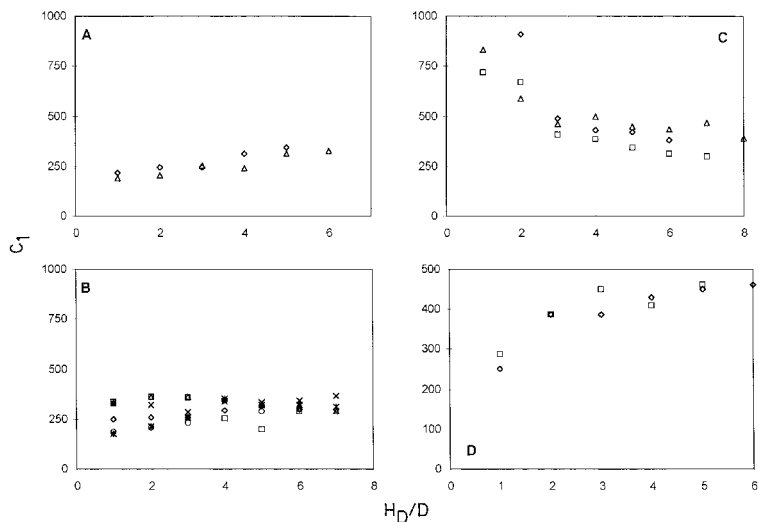


Figure 13.  $C_1$  versus  $H_D/D$  for various sparger designs for air-water system: (A)  $d_o < 1$  mm:  $\diamond$  SP1,  $\Delta$  SP11; (B)  $2.5 \text{ mm} \leq d_o \leq 6$  mm:  $\diamond$  SP3,  $\square$  SP4,  $\Delta$  SP13, X SP14, \* SP16,  $\circ$  SP17; (C) single point spargers,  $\diamond$  SP6,  $\square$  SP15,  $\Delta$  SP19; (D)  $d_o = 1.5$  mm,  $\diamond$  SP2,  $\square$  SP12.

- (i) generation of suitable grid system
- (ii) conversion of governing equations into algebraic equations
- (iii) selection of discretization schemes
- (iv) formulation of the discretized equation at every grid location
- (v) formulation of pressure equation
- (vi) development of a suitable iteration scheme for obtaining a final solution.

A finite control volume technique of Patankar<sup>18</sup> was employed for the solution of these equations. A staggered grids arrangement proposed by Patankar and Spalding<sup>19</sup>, consisted of  $10 \times 80$  grid points with 10 grid points in the radial direction and 80 grid points in the axial direction. The power law scheme was used for the discretization of the equations while the pressure velocity coupling was solved by the SIMPLE algorithm. The set of algebraic equations obtained after discretization were solved by

TDMA. Relaxation parameters and internal iterations for the variables were tuned to optimize the balance between the convergence criteria ( $1.0 \times 10^{-3}$ ) and the number of iterations required.

#### Correspondence Between the Real Systems and Predicted Flow

The comparison between the real systems and the predicted flow was done for three spargers SP11, SP13, and SP15. The superficial gas velocity ( $V_G$ ) was taken constant at  $295 \text{ mm s}^{-1}$ , and the  $H_D/D$  ratio was varied from 1 to 7.

The flow pattern mainly depends upon the superficial gas velocity ( $V_G$ ), column diameter and the nature of the gas liquid system. The last parameter is the most complex and its role cannot be predicted with the present status of knowledge. Therefore, a gas-liquid system is characterized by the drift flux model of Zuber and Findlay<sup>17</sup> and does not consider the liquid phase flow pattern within the column.

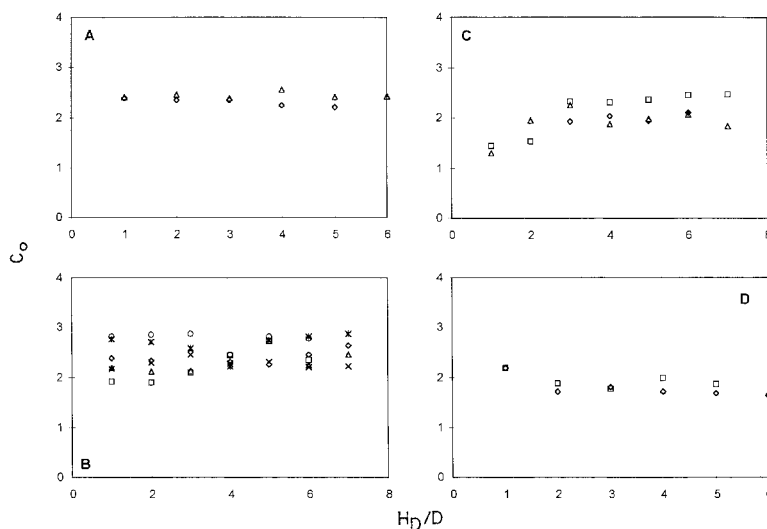


Figure 14.  $C_o$  versus  $H_D/D$  for various sparger designs for air-water system: (A)  $d_o < 1$  mm:  $\diamond$  SP1,  $\Delta$  SP11; (B)  $2.5 \text{ mm} \leq d_o \leq 6$  mm:  $\diamond$  SP3,  $\square$  SP4,  $\Delta$  SP13, X SP14, \* SP16,  $\circ$  SP17; (C) single point spargers,  $\diamond$  SP6,  $\square$  SP15,  $\Delta$  SP19; (D)  $d_o = 1.5$  mm,  $\diamond$  SP2,  $\square$  SP12.

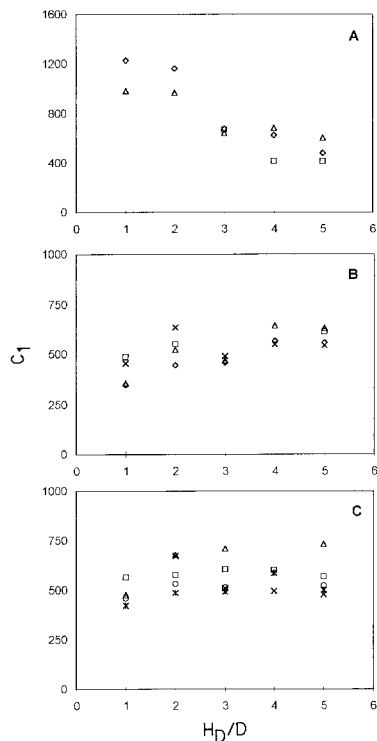


Figure 15.  $C_1$  versus  $H_D/D$  for various sparge designs for air-CMC solution system: (A) single point spargers,  $\diamond$  SP6,  $\square$  SP15,  $\Delta$  SP19; (B)  $d_o \leq 1.5$  mm,  $\diamond$  SP1,  $\square$  SP2,  $\Delta$  SP11, X SP12; (C)  $2.5$  mm  $\leq d_o \leq 6$  mm,  $\square$  SP13,  $\Delta$  SP14, X SP16, \* SP17,  $\circ$  SP18.

This necessitates a modification in the formulation of constants  $C_0$  and  $C_1$  as given by:

$$C_{OM} = \frac{\langle \varepsilon_G u_G \rangle}{\langle \varepsilon_G \rangle \langle V_S \rangle} + \frac{\langle -\varepsilon_G \varepsilon_L u_L \rangle}{\langle \varepsilon_G \rangle \langle u_G \rangle} \quad (5)$$

$$C_{IM} = \frac{\langle \varepsilon_G \varepsilon_L V_S \rangle}{\langle \varepsilon_G \rangle} + \frac{\langle -\varepsilon_G \varepsilon_L u_L \rangle}{\langle \varepsilon_G \rangle} \quad (6)$$

where  $u_z$  is the axial component of liquid velocity. It is important to understand whether the circulation affects the hold-up profile (Equation (5)) or the bubble rise velocity (Equation (6)). Therefore, the radial profiles of gas hold-up, true gas velocity ( $v_z$ ) and true liquid velocity ( $u_z$ ) were obtained using CFD simulation. These profiles were used for the estimation of  $C_0$  and  $C_1$ . In all cases, it was found that the liquid circulation must be included in the constant  $C_0$ . The comparison of predicted and experimental values of  $C_0$  and  $C_1$  are given in Table 3.

It can be seen that the agreement is excellent even for three different designs of the spargers. It can also be seen that the CFD predictions of the average gas hold-up are also excellent.

The combined effects of plate geometric parameters viz.,  $d_o$ ,  $P$ , and  $N$  on  $C_0$  of the drift flux model has been shown in Figure 17. For this, a distributor parameter as defined by Tsuchiya and Nakanishi<sup>3</sup> has been used as the x-axis ( $\eta_D$ ),  $H_D/D$  being the variable parameter.

The  $\bar{\varepsilon}_G - V_G$  data were also analysed for the transition from homogeneous regime to heterogeneous regime. It was observed that the transition gas hold-up is in the range of 9–22%. Under otherwise similar conditions of sparger design and  $H_D/D$  ratio, the value of  $\bar{\varepsilon}_{GC}$  was found to be the

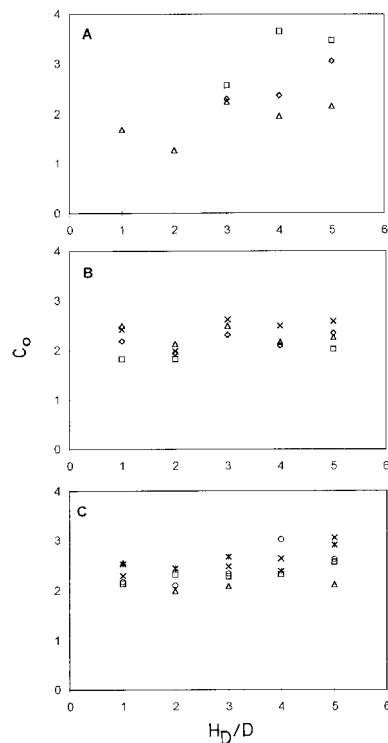


Figure 16.  $C_0$  versus  $H_D/D$  for various sparger designs for air-CMC solution system: (A) single point spargers,  $\diamond$  SP6,  $\square$  SP15,  $\Delta$  SP19; (B)  $d_o \leq 1.5$  mm,  $\diamond$  SP1,  $\square$  SP2,  $\Delta$  SP11, X SP12; (C)  $2.5$  mm  $\leq d_o \leq 6$  mm,  $\square$  SP13,  $\Delta$  SP14, X SP16, \* SP17,  $\circ$  SP18.

least for the air-CMC solution and the largest for the air-salt solution. For the air-water system, the  $\bar{\varepsilon}_{GC}$  was in between the air-CMC solution and the air-salt solution.

## CONCLUSIONS

- (1) The combined effect of sparger design and column height on the fractional gas hold-up was investigated. With an increase in the height to diameter ( $H_D/D$ ) ratio, the hold-up was found to decrease when multipoint spargers (with hole diameter  $< 3$  mm) were used. In contrast, for single-point spargers,  $\bar{\varepsilon}_G$  was found to increase. However, in both the cases, a limiting  $H_D/D$  ratio was observed beyond which the values of  $\bar{\varepsilon}_G$  remain practically constant.
- (2) The above observations were found to hold for three gas-liquids systems:
  - (i) air-water
  - (ii) relatively less coalescing system air-aqueous solution of electrolyte and
  - (iii) relatively more coalescing system air-aqueous solution of carboxymethyl cellulose (CMC).
- (3) The limiting value of the  $H_D/D$  ratio (beyond which  $\bar{\varepsilon}_G$  is independent of  $H_D/D$ ) was found to be in the range of 4–5 for the air-water system, greater than 8 for the air-electrolyte system and 3 for the air-aqueous CMC system.
- (4) The  $\bar{\varepsilon}_G$  versus  $V_G$  data was analysed using the Zuber and Findlay drift flux model. A predictive procedure has been developed for the drift constants on the basis of simulation using computational fluid dynamics. An excellent agreement has been shown between the CFD predictions and the experimental values of drift flux constants.

Table 2. Governing equations for the simulation in bubble column.

The governing equations written in a general form:

$$\frac{\partial}{\partial t}(\varepsilon\rho\Phi)_k + \frac{1}{r}\frac{\partial}{\partial r}(r\varepsilon\rho u\Phi)_k + \frac{\partial}{\partial z}(\varepsilon\rho u\Phi)_k = \frac{1}{r}\frac{\partial}{\partial r}\left(r\Gamma\varepsilon\rho u\frac{\partial\Phi}{\partial r}\right)_k + \frac{\partial}{\partial z}\left(\Gamma\varepsilon\rho u\frac{\partial\Phi}{\partial z}\right)_k + S_\Phi$$

Conservation of	$\Phi$	$\sigma_\Phi$	$\sigma_j$	$S_\Phi =$ source terms
Mass	1	$\infty$	1 to $\infty$	$\frac{1}{r}\frac{\partial}{\partial r}\left(r\mu_{i,k}\frac{\partial\varepsilon_k}{\partial r}\right) + \frac{\partial}{\partial z}\left(\mu_{i,k}\frac{\partial\varepsilon_k}{\partial z}\right)$
Axial component	$u$	1.0	1 to $\infty$	$-\varepsilon_G\frac{\partial P}{\partial z} + \varepsilon_G g + F_{dz} + F_{vz} + \left(\frac{1}{r}\frac{\partial}{\partial r}\left(r\varepsilon_G\mu_{i,G}\frac{\partial v_r}{\partial z}\right) + \frac{\partial}{\partial z}\left(\varepsilon_G\mu_{i,G}\frac{\partial v_z}{\partial z}\right)\right) + v_z\left(\frac{1}{r}\frac{\partial}{\partial r}\left(r\frac{\mu_{i,G}}{\sigma_j}\frac{\partial\varepsilon_G}{\partial r}\right)\right) + \frac{\partial}{\partial z}\left(\frac{\mu_{i,G}}{\sigma_j}\frac{\partial\varepsilon_G}{\partial z}\right) + \left(\frac{\mu_{i,G}}{\sigma_j}\frac{\partial\varepsilon_G}{\partial z}\right)\left(\frac{1}{r}\frac{\partial}{\partial r}(rv_r) + \frac{\partial v_z}{\partial z}\right)$
Radial component	$v_r$	1.0	1 to $\infty$	$-\varepsilon_G\frac{\partial P}{\partial r} + \varepsilon_G g - F_{dr} - F_{vr} - F_{lr} + \left(\frac{1}{r}\frac{\partial}{\partial r}\left(r\varepsilon_G\mu_{i,G}\frac{\partial v_r}{\partial r}\right) + \frac{\partial}{\partial z}\left(\varepsilon_G\mu_{i,G}\frac{\partial v_z}{\partial r}\right)\right) - 2\varepsilon_G\mu_{i,G}\frac{v_r}{r^2} + v_r\left(\frac{1}{r}\frac{\partial}{\partial r}\left(r\frac{\mu_{i,G}}{\sigma_j}\frac{\partial\varepsilon_G}{\partial r}\right)\right) + \frac{\partial}{\partial z}\left(\frac{\mu_{i,G}}{\sigma_j}\frac{\partial\varepsilon_G}{\partial z}\right) + \left(\frac{\mu_{i,G}}{\sigma_j}\frac{\partial\varepsilon_G}{\partial z}\right)\left(\frac{1}{r}\frac{\partial}{\partial r}(rv_r) + \frac{\partial v_z}{\partial z}\right)$
Turbulent Kinetic Energy	$k$	1.0	-	$\varepsilon_L(G + P_B - \rho_L\varepsilon)$
Turbulent Dissipation Energy	$\varepsilon$	1.3	-	$\varepsilon_L\frac{\varepsilon}{k}(C_{e1}G - C_{e2}\rho_L\varepsilon)$

where,  $\Gamma = \mu_{eff,k}/\sigma_\Phi$ ,  $\mu_{i,k} = 0.09\rho_k(k^2/\varepsilon)$ ,  $k =$  phase  $\mu_{eff,k} = \mu_{i,k} + \mu_k$ ,  $F_{lk} =$  Lift force  $F_{dk} =$  Friction force  $F_{vk} =$  Virtual mass force

$$P_b = C_B[F_{dr}V_{Sr} + F_{dz}V_{Sz}]$$

$$G = \mu_{i,L}\left[\left(\frac{\partial u_r}{\partial r}\right)^2 + \left(\frac{u_r}{r}\right)^2 + \left(\frac{\partial u_z}{\partial z}\right)^2 + \left(\frac{\partial u_r}{\partial z} + \frac{\partial u_z}{\partial r}\right)^2\right]$$

\* Force terms are positive for liquid phase and negative for gas phase

Table 3A. Comparison between the predicted and experimental results for the sparger SP11,  $V_G = 295 \text{ mm s}^{-1}$ ,  $D = 0.385$ .

$H_b/D$	$V_G$ predicted	$\varepsilon_G$		$C_o$		$C_1$		$V_c$
		predicted	exptl.	predicted Equation (5)	exptl.	predicted Equation (4)	exptl.	
2	0.295	0.315	0.319	2.463	2.457	0.259	0.205	1.257
3	0.295	0.301	0.305	2.401	2.387	0.281	0.255	1.220
4	0.295	0.298	0.298	2.520	2.550	0.273	0.240	1.243
5	0.295	0.280	0.283	2.402	2.403	0.332	0.311	1.005
6	0.295	0.278	0.280	2.419	2.426	0.347	0.236	0.990

Table 3B. Comparison between the predicted and experimental results for the sparger SP13,  $V_G = 295 \text{ mm s}^{-1}$ ,  $D = 0.385$ .

$H_b/D$	$V_G$ predicted	$\varepsilon_G$		$C_o$		$C_1$		$V_c$
		predicted	exptl.	predicted Equation (5)	exptl.	predicted Equation (4)	exptl.	
2	0.295	0.293	0.305	2.22	2.11	0.355	0.360	0.611
3	0.295	0.305	0.304	2.11	2.13	0.360	0.362	0.596
4	0.295	0.290	0.290	2.65	2.73	0.245	0.225	1.222
5	0.295	0.354	0.280	2.12	2.94	0.224	0.187	1.054

Table 3C. Comparison between the predicted and experimental results for the sparger SP5,  $V_G = 295 \text{ mm s}^{-1}$ ,  $D = 0.385$ .

$H_D/D$	$V_G$ predicted	$\varepsilon_G$		$C_O$		$C_1$		$V_C$
		predicted	exptl.	predicted Equation (5)	exptl.	predicted Equation (4)	exptl.	
4	0.295	0.269	0.275	2.33	2.31	0.397	0.305	0.95
5	0.295	0.276	0.281	2.42	2.37	0.358	0.343	0.975
6	0.295	0.281	0.283	2.464	2.45	0.326	0.312	1.024
7	0.295	0.283	0.285	2.492	2.47	0.314	0.298	1.028

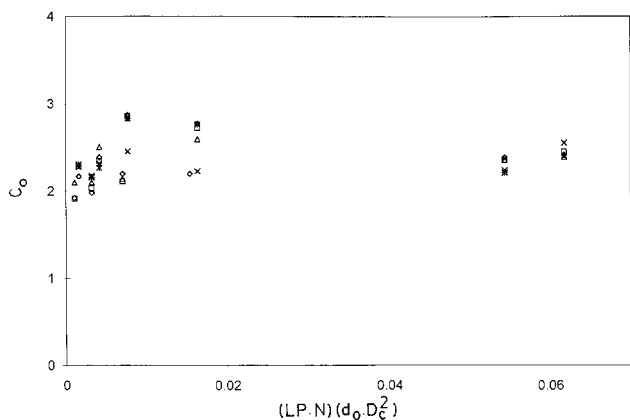


Figure 17.  $C_O$  versus distributor parameter,  $\eta_p$ , with  $H_D/D$  as a parameter for air-water system:  $\diamond$   $H_D/D = 1$ ,  $\square$   $H_D/D = 2$ ,  $\Delta$   $H_D/D = 3$ ,  $\times$   $H_D/D = 4$ ,  $*$   $H_D/D = 5$ .

(5) A relationship has been given between  $C_O$  and the geometric parameters, as shown in Figure 17.

## NOMENCLATURE

$C_B$	interface energy transfer factor
$C_D$	drag force coefficient
$C_L$	lift force coefficient
$C_O, C_1$	drift flux model constants as defined by equations (3) and (4), respectively
$C_{OM}, C_{IM}$	modified Drift flux model constants as defined by equations (5) and (6), respectively
$C_{mans}$	transition concentration of electrolyte solution, M
$C_V$	virtual mass force coefficient
$C_{\varepsilon 1}$	model parameter in turbulent dissipation energy equation (= 1.44)
$C_{\varepsilon 2}$	model parameter in turbulent dissipation energy equation (= 1.92)
$D$	diameter of column, m
$d_{BP}$	primary bubble size, mm
$d_{BS}$	secondary bubble size, mm
$d_o$	hole diameter, mm
F.A.	free area of sparger, %
$F_{DR}$	friction force in radial direction = $C_D \varepsilon_L \varepsilon_G (v_G - v_L)$
$F_{DZ}$	friction force in axial direction = $C_D \varepsilon_L \varepsilon_G (u_G - u_L)$
$F_1$	lift force = $C_L \varepsilon_L \varepsilon_G \rho_L (u_G - u_L)$
$F_{VR}$	virtual mass force in radial direction = $C_V \varepsilon_L \varepsilon_G \rho_L \left[ \frac{1}{r} \frac{\partial}{\partial r} r (v_G - v_L) + \frac{\partial}{\partial z} (v_G - v_L) \right]$
$F_{VZ}$	virtual mass force in axial direction = $C_V \varepsilon_L \varepsilon_G \rho_L \left[ \frac{\partial}{\partial r} (u_G - u_L) + \frac{\partial}{\partial z} (u_G - u_L) \right]$
$G$	= $\mu_{i,L} 2 \left[ \left( \frac{\partial v_L}{\partial r} \right)^2 + \left( \frac{v_L}{r} \right)^2 + \left( \frac{\partial u_L}{\partial z} \right)^2 \right] + \left[ \left( \frac{\partial v_L}{\partial z} \right)^2 + \left( \frac{\partial u_L}{\partial r} \right)^2 \right]$
$g$	gravitational constant, $\text{m s}^{-2}$
$H$	height of clear liquid in bubble column, m

$H_D$	height of gas dispersion, m
$k$	consistency index of the power law model, $\text{mPa s}^n$
$k$	turbulent kinetic energy, $\text{m}^2 \text{s}^{-2}$
$n$	flow behaviour index
$N$	number of holes
$P$	pressure, $\text{N m}^{-2}$
$P_b$	= $C_b [F_{dr} V_{Sr} + F_{dz} V_{ze}]$
$u_G$	axial component of gas velocity, $\text{mm s}^{-1}$
$u_L$	axial component of liquid velocity, $\text{mm s}^{-1}$
$V_C$	liquid circulation velocity, $\text{mm s}^{-1}$
$V_G$	superficial gas velocity, $\text{mm s}^{-1}$
$v_G$	radial component of gas velocity, $\text{m s}^{-1}$
$v_L$	radial component of liquid velocity, $\text{m s}^{-1}$
$V_S$	axial slip velocity between gas and liquid $\text{m s}^{-1}$

## Greek letters

$H_K$	$\mu_K + \mu_{i,K} \sigma_\phi$
$\mu_K$	molecular viscosity of phase $K = 0.09 \rho_K (k^2/\varepsilon)$
$\mu_K$	turbulent viscosity of phase $K$
$\nu$	molecular kinematic viscosity of liquid
$\nu_i$	turbulent kinematic viscosity of liquid
$\sigma$	surface tension, $\text{N m}^{-1}$
$\sigma_\phi$	turbulent Prandtl number for $H$ term in Table 2
$\sigma_f$	turbulent Prandtl number for source terms in Table 2
$\eta_p$	distributor parameter, $(LP.N)/(d_o.D_c^2)$
$\bar{\varepsilon}_G$	average fractional hold up
$\varepsilon_G$	fractional hold up
$\varepsilon_{GC}$	critical value of average fractional hold up

## Subscripts

$G$	gas phase
$K$	phase, $K = G$ gas phase, $K = L$ liquid phase
$L$	liquid phase

## REFERENCES

- Freedman, W. and Davidson, J. F., 1969, Hold-up and liquid circulation in bubble columns, *Trans IChemE*, 47: 251–262.
- Zahradnik, J. and Kastanek, F., 1979, Gas hold-up in uniformly aerated bubble column reactors, *Chem Eng Commun*, 3: 413.
- Tsuchiya, K. and Nakanishi, O., 1992, Gas hold-up behavior in a tall bubble column with perforated plate distributors, *Chem Eng Sci*, 47: 3343–3354.
- Takahashi, T., Miyahara, T. and Shimizu, K., 1974, Experimental studies of gas void fraction and froth height on a perforated plate- low clear liquid height under liquid stagnant flow, *J Chem Eng Japan*, 7: 75.
- Gopal, J. S. and Sharma, M. M., 1983, Mass transfer characteristics of low H/D bubble columns, *Can J Chem Eng*, 61: 517–526.
- Kawagoe, K., Inoue, T., Nakao, K. and Otake, T., 1976, Flow pattern and gas hold-up conditions in gas sparged contactors, *Int Chem Eng*, 16: 176–184.
- Voigt, J. and Schugerl, K., 1979, Absorption of oxygen in counter-current multistage bubble columns-I, *Chem Eng Sci*, 34: 1221–1229.
- Oels, U., Lucke, J., Buchholz, R. and Schugerl, K., 1978, Influence of gas distributor type and composition of liquid on the behavior of a bubble column bioreactor, *Ger Chem Eng*, 1: 115–129.
- Herbard, G., Bastoul, D. and Roustan, M., 1996, Influence of the gas sparger on the hydrodynamic behaviour of bubble columns, *Trans IChemE*, 74(A): 406–414.
- Bach, H. F. and Pihlofer, T., 1978, Variation of gas hold-up in bubble columns with physical properties of liquid and operating conditions of columns, *Ger Chem Eng*, 1: 270.

11. Ohki, Y. and Inoue, H., 1970, Longitudinal mixing of the liquid phase in bubble columns, *Chem Eng Sci*, 25: 1–16.
12. Wilkinson, P. M., 1991, Physical aspects and scale-up of high pressure bubble columns, *PhD Thesis*, (University of Groningen, NL).
13. Botton, R., Cosserat, D. and Charpentier, J. F., 1978, Influence of column diameter and High gas throughputs on the operation of a bubble column, *Chem Eng J*, 16: 107–114.
14. Kawasaki, H. and Tanaka, H., 1996, Correlation of volumetric mass transfer coefficient with gas hold-up in the calming section in a bubble column with a single hole orifice, *J Chem Eng Japan*, 29(2): 365–367.
15. Miyahara, T., Matsuuba, Y., Kaseno, S. and Takahashi, T., 1982, Gas hold-up on a perforated plate, *J Chem Eng Japan*, 15(5): 391.
16. Zahradnik, J., Fialova, M., Kastanek, F., Green, K. D. and Thomas, N. H., 1995, The effect of electrolytes on bubble coalescence and gas hold-up in bubble column reactors, *Trans IChemE*, 73(A): 341–346.
17. Zuber, N. and Findlay, J. A., 1965, Average volumetric concentration in two phase flow systems, *J Heat Trans*, 87, 453.
18. Patankar, S. V., 1980, *Numerical Heat Transfer and Fluid Flow*, (McGraw Hill, New York).
19. Patankar, S. V. and Spalding, D. B., 1972, A calculation procedure for heat, mass and momentum transfer in three dimensional parabolic flows, *Int J Heat Mass Transfer*, 15: 1787.

#### ADDRESS

Correspondence concerning this paper should be addressed to Professor J. B. Joshi, Department of Chemical Technology, University of Mumbai, Matunga, Mumbai 400 019, India.

*The manuscript was received 15 January 1998 and accepted for publication after revision 26 June 1998.*